2026 IEEE International Conference on Robotics and Automation (ICRA 2026)
June 1-5, 2026. Vienna, Austria

UVDtact: UV Marker-Embedded Fingertip-Like Vision-Based Tactile Sensor for Shape Reconstruction and Force Estimation

Woojong Kim, Won Dong Kim, Hyunkyu Park, Joonho Lee, Jeong-Jung Kim, and Jung Kim

***Abstract*— Vision-based tactile sensors are highly promising for enabling robots to perform dexterous, contact-rich manipulation tasks by providing high-resolution tactile data. Recent studies have attempted to implement shape reconstruction and force estimation capabilities for sensors with omnidirectional sensing surfaces and a compact form factor. However, achieving a small diameter comparable to that of a human fingertip remains challenging, and integrating the multiple functionalities within the fingertip form factor poses significant challenges. In this study, we present UVDtact, a vision-based tactile sensor with a fingertip-like form factor that incorporates a switchable translucent elastomer. The proposed switchable translucent elastomer, which integrates ultraviolet (UV) ink and a translucent elastomer, decouples tactile images for shape reconstruction and force estimation. The independent tactile images ensure that shape reconstruction remains unaffected by UV markers, making them visible when needed, thereby enabling effective force estimation. For shape reconstruction, we leverage the darkening effect of the translucent elastomer in response to tactile stimuli and introduce a calibration method that utilizes this effect in an all-around curved sensor configuration. Furthermore, we validate that embedding UV markers enhances tactile features, improving force estimation performance while preserving the quality of tactile images used for shape reconstruction. By integrating various tactile sensing capabilities into a compact, fingertip-like design, UVDtact contributes to developing robotic systems with human-like dexterity.**

I. Introduction

Tactile perception is essential for humans to perceive and interact with their environment. The dense arrangement of tactile receptors in the skin enables humans to gather various tactile information, such as the shape, texture, and contact force of objects, facilitating object recognition, grasping, assembly, and tool manipulation [1], [2]. Similarly, robots require tactile sensors with high-fidelity tactile imaging to achieve delicate and contact-rich manipulation [3], [4]. To this end, various tactile sensors have been developed by arranging elements based on different transducing methods, such as piezoelectric [5], resistive [6], and capacitive [7] principles, in an array format [8]. However, these solutions often face limitations such as high costs and complex manufacturing processes.

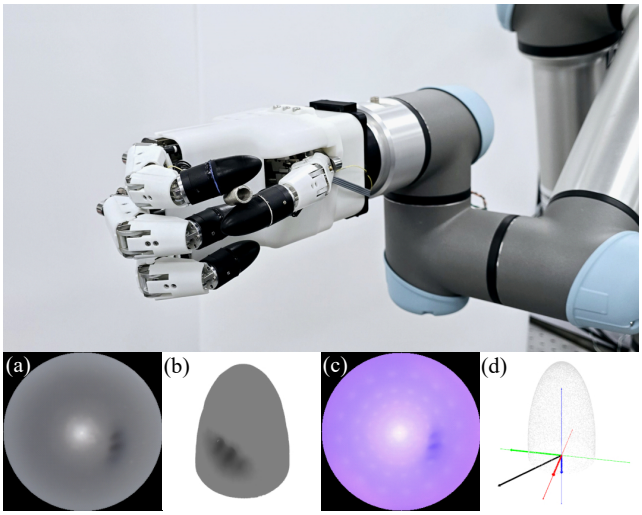

Fig. 1. UVDtact sensors mounted on an anthropomorphic robotic hand [9] holding a spring. (a) Tactile image captured from the sensor at the thumb position in white LED mode. (b) Corresponding shape reconstruction result. (c) Tactile image captured from the same sensor in UV LED mode. (d) Visualization of the force estimation result.

Vision-based tactile sensors have recently gained popularity by embedding a miniature camera within the sensor to obtain high-resolution tactile information in a straightforward manner [10], [11]. To approach the human skin's ability to recognize the shape of an object and the force with which it interacts, various vision-based tactile sensors, including prominent examples such as GelSight [12] and TacTip [13], have been developed. Additionally, a range of algorithms has been proposed to implement the functions of surface reconstruction and force estimation using high-resolution tactile images [14]–[22]. More recently, advancements have led to the development of compact designs, such as GelSlim 3.0 [23], DelTact [24], and 9DTact [25], which can perform both functions without replacing the elastomer. However, despite their functionality and compactness, the limited form factor of a flat sensing surface may not be suitable for common manipulation tasks that can be performed by the human hand.

The design of vision-based tactile sensors is advancing toward the form factor of a human fingertip with an all-around shape. This design is beneficial for effectively manipulating a variety of tools designed to match the shape of the human fingertip and is essential for replicating human-like dexterity

This work was supported in part by the National Research Council of Science and Technology as part of the project titled "Development of core technologies for robot general purpose task artificial intelligence (RoGeTA) framework" under Grant NK261B. *(Corresponding author: Jung Kim.)*

W. Kim, W. D. Kim, H. Park, J. Lee, and J. Kim are with the Department of Mechanical Engineering at KAIST, Daejeon 34141, Republic of Korea (e-mail: kwjong2028@kaist.ac.kr; kwd92@kaist.ac.kr; hkpark93@kaist.ac.kr; joonholee@kaist.ac.kr; jungkim@kaist.ac.kr)

J. Lee and J.-J. Kim are with the Korea Institute of Machinery and Materials, Daejeon 34103, Republic of Korea (e-mail: joonholee@kimm.re.kr, rightcore@kimm.re.kr).

in robotic systems. To achieve this, various all-around vision-based tactile sensors capable of omnidirectional sensing, such as DenseTact 2.0 [26], Minsight [27], GelSight360 [28], AllSight [29], and RainbowSight [30], have been recently developed. However, existing designs still exhibit considerably large diameters due to the size of the embedded camera and its field of view. Furthermore, achieving both key functionalities, shape reconstruction and force estimation, at such form factors has remained challenging.

Here, we present UVDtact (Fig. 1), a vision-based tactile sensor with a fingertip-like form factor design that incorporates a switchable translucent elastomer. The proposed switchable translucent elastomer, which integrates ultraviolet (UV) ink and a translucent elastomer, decouples tactile images for shape reconstruction and force estimation. The independent tactile images ensure that shape reconstruction remains unaffected by UV markers, making them visible when needed, thereby enabling effective force estimation. For shape reconstruction, we leverage the darkening effect of a translucent elastomer under tactile stimulation and propose a calibration method that utilizes this effect in an all-around curved sensor configuration. Additionally, UV markers enrich tactile features, further improving force estimation. Performance evaluations were conducted to assess the shape reconstruction and force estimation capabilities, demonstrating an error of 0.172 mm for shape reconstruction and 0.120 N for force estimation. To highlight the effectiveness of the sensor design, sensors with fewer or no markers were fabricated and compared. Experimental results showed that integrating UV markers reduces force estimation error by approximately 60 % compared to configurations without UV markers, while preserving the quality of tactile images used for shape reconstruction.

The paper is organized as follows. After the introduction, Section II reviews related works. Section III presents the sensor design of UVDtact, and Section IV presents methods for shape reconstruction and force estimation. Section V shows experimental results, and the conclusion and future work are discussed in Section VI.

II. Related works

With advancements in image sensors and computer vision technologies, vision-based tactile sensors have gained popularity for providing high-resolution tactile information. These sensors typically operate by tracking changes in images caused by tactile stimuli, employing a camera placed inside a soft elastomer [10], [11]. The captured tactile images enable the extraction of various tactile features, such as detailed surface geometry, as well as normal and shear contact forces.

One of the popular examples, GelSight [12] utilizes photometric stereo techniques to reconstruct the shape of the sensing surface. Similar to TacTip [13], GelForce [31], FingerVision [32], and other sensors that rely on marker information, GelSight also incorporated markers placed on an elastomer membrane from its early versions to extract marker motion information [12]. Gelslim 3.0 achieved shape reconstruction and force map estimation in a compact form by combining photometric stereo with marker information [23]. However, the areas occupied by black markers cannot be used for shape reconstruction, leading to a decrease in shape reconstruction performance, which has been attempted to be addressed through interpolation methods [33].

TABLE I

Comparison of all-around vision-based tactile sensors

Sensor	Elastomer size (mm)	Contact features
DenseTact 2.0 [26]	ϕ 32 × 16	Shape, Force
Minsight [27]	ϕ 22 × 30	Contact location, Force map
GelSight360 [28]	ϕ 28 × 29.5	Shape
AllSight [29]	ϕ 24 × 26	Contact location, Force
RainbowSight [30]	ϕ 20 × 21.5	Shape
Digit Pinki [34]	ϕ 15 × 16	Contact area, Force
UVDtact (ours)	ϕ 18 × 24	Shape, Force

Note: The comparison was conducted only on the latest sensors developed after 2023.

To address these issues, tactile sensors utilizing various principles have been developed recently. Our previous work, UVtac [16] used UV-reactive fluorescent inks (UV ink) to achieve effective force estimation and object localization. DelTact utilized densely arranged color patterns on the elastomer, instead of sparsely placed markers, and employed dense optical flow and natural Helmholtz-Hodge decomposition to achieve shape reconstruction and force map estimation [24]. 9Dtact utilized the phenomenon of a translucent elastomer darkening with contact to perform shape reconstruction and implemented force estimation using a dense gel flow [25]. While these sensors have achieved multifunctionality and compact form factors, their flat sensing surface may not be suitable for general manipulation tasks.

Recent developments have advanced beyond flat sensing surfaces, proposing various sensors with all-around shapes and trending toward smaller diameters that approximate human finger sizes. The Minsight sensor [27], similar to its predecessor Insight [35], utilizes photometric stereo and structured light to achieve contact location estimation and force mapping in a compact size. However, using an internal skeleton limits the contact force to within 2 N. DenseTact 2.0 [26], building on DenseTact [36], enhances tactile features with randomized patterns and simultaneously achieves shape reconstruction and force estimation. Nonetheless, using a hemispherical elastomer without a rigid structure may affect durability. AllSight [29] offers a low-cost, easy-to-manufacture solution that achieves contact location estimation and force estimation, utilizing the TACTO simulator for data efficiency. GelSight360 [28] and RainbowSight [30] each utilize a crossed LED PCB and rainbow illumination strategy to apply photometric stereo technology to the all-around shape sensor and achieve shape reconstruction. The recently presented Digit Pinki [34] achieved the smallest diameter by utilizing fiber optic bundles, but it involves a bulky imaging and illumination system outside the sensing elastomer.

Table 1 provides a comparative summary of all-around vision-based tactile sensors, highlighting their sizes and functionalities. Although all-around vision-based tactile sensors have made significant strides through the aforementioned studies, achieving a human fingertip-like form factor along

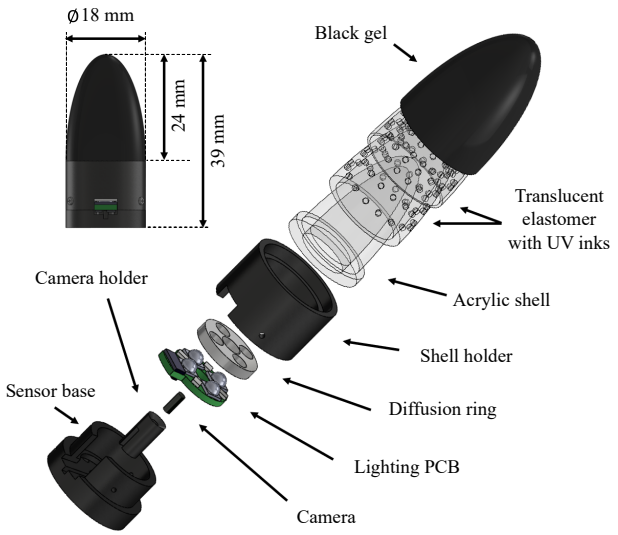

Fig. 2. Exploded view of UVDtact sensor.

with shape reconstruction and force estimation remains challenging.

III. Design and Fabrication

A. Design Criteria

The design criteria of UVDtact, aimed at achieving both shape reconstruction and force estimation within a human fingertip-like form factor, are as follows: 1) The sensor should have a size comparable to that of a human fingertip and feature an all-around 3D sensing surface. 2) An elastomer design, fabrication process, and algorithms should be devised to achieve effective shape reconstruction and force estimation. 3) The sensor must be easy to manufacture, durable, and designed such that all components, except the wires for powering the LEDs and transmitting image data from the camera, are housed inside the sensor.

To meet these criteria, the shape of the elastomer, which determines the sensing surface, was designed as a half-ellipsoid shape with a diameter of 18 mm and a height of 24 mm, based on the diameter [37] and surface area [38] of a human index fingertip. Additionally, UV ink and a translucent elastomer were utilized to embed tactile image features that effectively support each function. Lastly, other components were carefully designed to ensure durability and ease of production. The structure and dimensions of the UVDtact sensor are illustrated in Fig. 2. In the following section, we describe the elastomer design developed to meet the criteria. This is followed by a description of the design choices and fabrication process for the detailed sensor components.

B. Switchable Translucent Elastomer Design

To achieve shape reconstruction and force estimation, we constructed a strategy to integrate the sensor features of UVtac [16] and DTact [17], which had flat sensing surfaces and applied them to an all-around sensor configuration. Our previous work, UVtac, utilized the switchable properties of UV ink to achieve effective force estimation under UV light while preserving the quality of tactile images under white light. Meanwhile, DTact demonstrated shape reconstruction by leveraging the reflective properties of a translucent elastomer using only white light without the need for RGB lighting. By combining the advantages of both sensors, we attempted to obtain separate tactile images for implementing shape reconstruction and force estimation by integrating switchable properties and the reflective characteristics of the translucent elastomer. The independent tactile images facilitate shape reconstruction by utilizing translucency while keeping the markers invisible, and they can enhance force estimation by incorporating marker-based features.

To realize this, we created a mixed elastomer by blending a translucent elastomer with UV ink, which displays color under UV light while maintaining translucency under white light. Additionally, to ensure that UV markers are visible in images captured by the camera due to color differences, we designed a two-layer structure of mixed elastomer using two different colors of UV ink. The two-layer mixed elastomer was set to a thickness of 2 mm, considering the sensor size, and each layer was designed with slots and protrusions. The inner mixed elastomer layer was designed with a baseline thickness of 1.5 mm and included slots corresponding to the number of markers, while the outer mixed elastomer layer had a baseline thickness of 0.5 mm and was designed with protrusions to fill the slots. The shapes of the slots and protrusions were designed as cylinders with a radius of 0.5 mm and a height of 0.5 mm, extended with hemispheres of 0.5 mm radius, considering ease of fabrication and the visibility of UV markers.

The colors of the two UV inks were carefully selected to ensure that the mixed elastomer maintains similar translucency under white light, preventing UV markers from being visible and preserving the quality of tactile images. Red and blue UV inks, which exhibited similar translucency in the mixed elastomer under white light, were chosen. The red UV ink was applied to the inner mixed elastomer layer, while the blue UV ink was used for the outer mixed elastomer layer. Lastly, to absorb internal light passing through the translucent elastomer layers, a 0.4 mm-thick black gel was placed around the outer edges of the mixed elastomer layers. As a result, we developed an all-around translucent elastomer design for shape reconstruction that appears darker in camera images under white light, depending on the degree of deformation. Additionally, the proposed switchable design enhances tactile features for force estimation by allowing the elastomer to darken based on the degree of deformation under UV light, while simultaneously making the movement of UV markers visible.

C. Details of the Components and Fabrication Process

Camera and Illumination system: Most compact vision-based tactile sensors utilize miniature cameras equipped with fisheye lenses and image sensors, such as the OV5647 and IMX219, to capture the entire sensing surface. However,

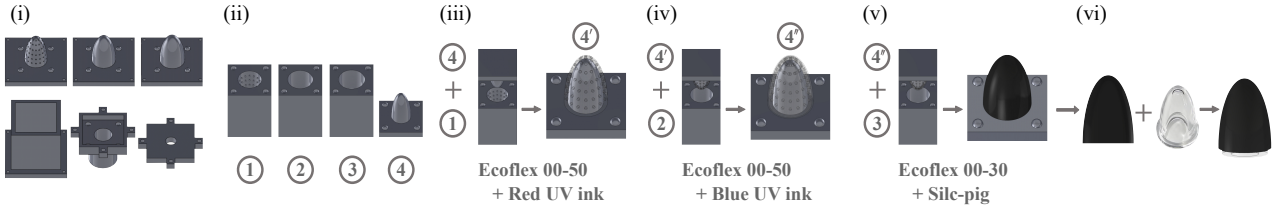

Fig. 3. The elastomer fabrication process of UVDtact. (i) Preparation of 3D-printed negative molds. (ii) Fabrication of silicone molds. (iii) Fabrication of inner mixed elastomer. (iv) Fabrication of outer mixed elastomer. (v) Fabrication of black gel. (vi) Merging the elastomer with the acrylic shell.

these cameras typically have a large diameter of over 10 mm, and the illumination system should be positioned outside this diameter, making it challenging to achieve the compactness of a human fingertip. To address this issue, we adopted a commercial endoscopic camera (muC103P, COMedia Ltd.) equipped with a CMOS image sensor (OVM6946, OmniVision), commonly used in medical applications. The adopted endoscopic camera features a highly compact size with a diameter of 1.5 mm and a height of 3 mm, providing a 120-degree field of view (FOV). A 0.5 mm wire connected to the camera transmits images to a desktop Universal Serial Bus (USB) port via a USB video processing board (C8209DP, COMedia Ltd.), allowing the desktop to stream 400×400 images at 30 fps.

For the illumination system, we designed a lighting printed circuit board (PCB) capable of switching between emitting UV light and white light. The lighting PCB consists of four white LEDs, four UV LEDs (with a peak wavelength of 365 nm), two resistors, and a dual Single Pole Single Throw (SPST) switch. The white and UV LEDs are alternately arranged every 45 degrees to ensure uniform illumination, with each forming separate parallel circuits connected to resistors. The switch is connected to a 5V power source and digital pins for controlling the white and UV LEDs in a manner similar to [16]. Using the GPIO pins of a Raspberry Pi board, the lighting mode can be switched between white and UV LED modes. Additionally, a white diffusion ring, fabricated using stereolithography (SLA) 3D printing, was designed to prevent over-reflections from the LEDs. However, since UV light does not pass through the diffusion ring effectively, holes were created in the areas corresponding to the UV LEDs, allowing UV light to directly reach the entire sensing surface.

Elastomer Fabrication: The elastomer is composed of two layers of mixed elastomer and a black gel, and it is fabricated sequentially, starting from the inner layer. Considering the manufacturability of the mixed elastomer with a slot-and-protrusion structure, we adopted a method utilizing negative molds, and the fabrication process begins by printing these molds using an SLA 3D printer (Form 3, Formlabs) (Fig. 3 (i)). Then, using the negative molds and Mold Star 30 (Smooth-On), silicone molds corresponding to the outer and inner boundaries of each layer are fabricated (Fig. 3 (ii)).

The materials for the inner mixed elastomer, which is the first to be fabricated using silicone molds, were selected as Ecoflex 00-50 (Smooth-On, shore 00 hardness 50) and water-based red UV ink (UV invisible ink, Ceres), considering translucency and sensor sensitivity. Once Ecoflex 00-50 Part A, Part B, and red UV ink are mixed in a ratio of 10:10:1 and degassed, the mixture is poured into the outer silicone mold, then combine the inner silicone mold with the outer mold to produce the inner mixed elastomer. After curing for 3 hours, the outer silicone mold is removed, and the inner mixed elastomer along with the inner silicone mold is used for the subsequent process (Fig. 3 (iii)).

The outer mixed elastomer is fabricated using the same mixing ratio and process as the inner mixed elastomer, with the only difference being that, among the materials, the red UV ink is replaced with blue UV ink (Fig. 3 (iv)). Subsequently, the black gel, which serves to absorb internal light and block external light, is fabricated using a mixture of Ecoflex 00-30 (Smooth-On, shore 00 hardness 30) Part A, Part B, and black Silc-Pig (Smooth-On) in a 5:5:1 ratio, following the same process (Fig. 3 (v)). After a curing time of 4 hours, silicone molds are removed from the elastomer. For sensor durability, a custom-fabricated transparent acrylic shell from JLCPCB was utilized to serve as a rigid internal skeleton. The acrylic shell is machined using computer numerical control (CNC) and finished with vapor polishing, and its half-ellipsoid section has a thickness of 2 mm, designed considering the camera's FOV. The fabrication process of the elastomer part is finalized by attaching this acrylic shell to the elastomer using clear silicone sealant (Fig. 3 (vi)).

Sensor Assembly: For the sensor assembly, the camera holder, shell holder, and sensor base are fabricated using an SLA 3D printer. As shown in Fig. 2, the sensor base, camera, camera holder, lighting PCB, and diffusion ring are arranged, and the components are secured to the sensor base using instant adhesive. Likewise, the acrylic shell of the elastomer part is attached to the shell holder with instant adhesive. To ensure the fixation and easy replacement of the elastomer, the sensor base and shell holder are fastened together with three M1.2 bolts, completing the sensor assembly.

IV. Shape Reconstruction and Force Estimation

In this section, we introduce the methods for shape reconstruction and force estimation of UVDtact. The sensor can switch between white LED mode and UV LED mode, performing shape reconstruction in white LED mode and force estimation in UV LED mode, as illustrated in Fig. 4. The following subsections provide a detailed explanation of

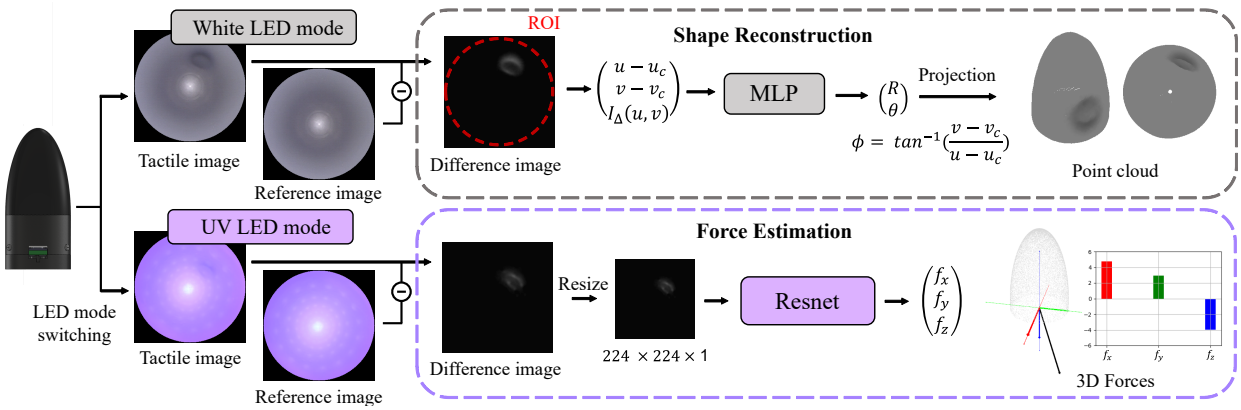

Fig. 4. Processing pipelines for the two core functionalities of UVDtact are illustrated. UVDtact utilizes learning-based methods for both shape reconstruction and force estimation. A reference image is captured when there is no contact on the sensor, while a tactile image is captured when an object presses against the sensor.

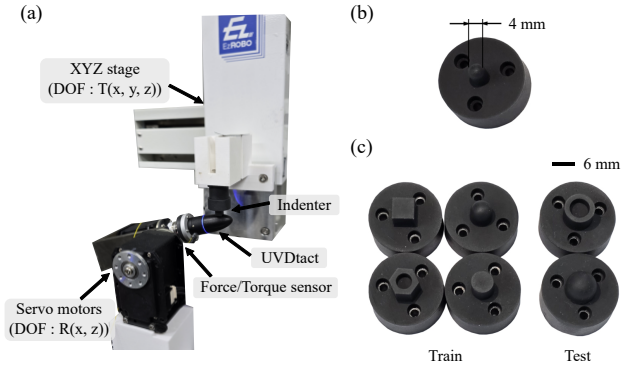

Fig. 5. (a) Data collection system, (b) Indenter used for the shape reconstruction dataset, (c) Indenters used for the force estimation dataset.

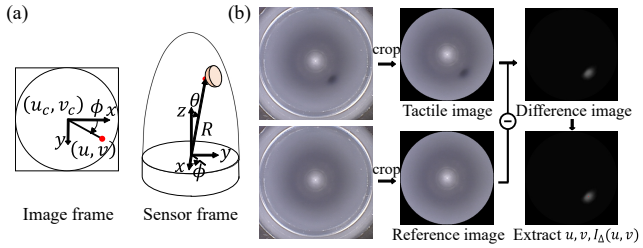

Fig. 6. (a) Image and sensor frame of the sensor, (b) Preprocessing procedure of the shape reconstruction dataset.

the data collection process, shape reconstruction, and force estimation methods for performing each function in the all-around sensor configuration.

A. Data Collection

The data collection system, as shown in Fig. 5 (a), comprises an XYZ stage (EzROBO-5GX, Iwashita Engineering, INC.), two servo motors (MX-64AT, Dynamixel), a force/torque (F/T) sensor (Nano 17, ATI), and indenters for pressing the sensor. The XYZ stage, equipped with the indenter, controls the indenter through Cartesian movement across three degrees of freedom while the two servo motors, to which the F/T sensor and UVDtact are attached, adjust the sensor's orientation (yaw and roll).

For the shape reconstruction dataset, a 3D-printed hemispherical indenter with a diameter of 4 mm (Fig. 5 (b)) was pressed in a normal direction onto the sensor surface to depths of up to 1.6 mm. The collected dataset consists of a total of 33,803 probing coordinates, comprising tactile images and reference images paired with the 3D coordinates of the indenter relative to the sensor.

For the force estimation dataset, six 3D-printed indenters of various shapes were utilized, as shown in Fig. 5 (c). After the indenter makes contact with the sensor surface in the normal direction at various positions, it applies normal and shear deformations to the sensor. The normal and shear deformations are applied up to a maximum of 1.4 mm, which exerts a force magnitude ($\|F\|$) of up to about 8 N on the sensor. The collected dataset includes 6,167 measurements per indenter, totaling 37,002 image-force pairs, each consisting of a measured force, a tactile image, and a reference image. For comparison of force estimation performance, sensors with fewer markers or without markers were also fabricated, and a dataset of 37,002 samples was collected for each sensor under the same deformation conditions.

B. Shape Reconstruction

The shape reconstruction of UVDtact is conducted in white LED mode following the pipeline shown in the top dashed box of Fig. 4. In white LED mode, the sensor exhibits a darkening characteristic in response to deformation, where the intensity variation value $I_\Delta(u, v)$ at a pixel position (u, v) is influenced by both the three-dimensional position resulting from the deformation and the pixel position (u, v). This relationship is nonlinear, making it difficult to derive an explicit inverse function. Therefore, an appropriate mapping method is required to estimate the 3D position using pixel positions and intensity variation values for shape reconstruction.

To address this, we first considered the all-around nature of the sensor and incorporated geometric relationships by computing the ϕ value in the spherical coordinate system (Fig. 6 (a)). Specifically, using the pixel coordinates (u_c, v_c) at the sensor's center, we directly com-

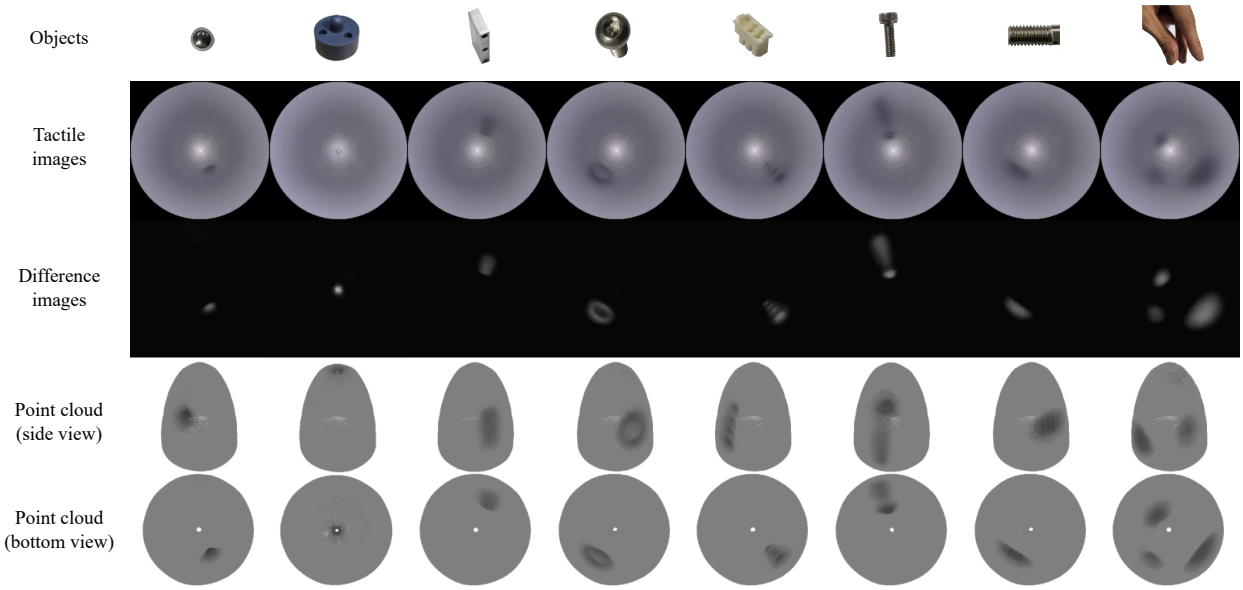

Fig. 7. Tactile signals collected when different objects are pressed at various locations on the UVDtact, along with the corresponding shape reconstruction results.

puted ϕ through a geometrically derived equation ($\phi = \tan^{-1}\left(\frac{v-v_c}{u-u_c}\right)$). Meanwhile, for the remaining two coordinates (R, θ), a data-driven approach using a multilayer perceptron (MLP) was employed to learn the nonlinear relationship. Through this method, shape reconstruction can be achieved while maintaining geometric consistency and accounting for nonlinear relationships. Similar to [17], which established a mapping list between intensity variation value and depth and applied it across the entire sensing surface, we applied this mapping to all pixels within the region of interest (ROI) on the sensing surface, resulting in a point cloud matching the pixel count of the ROI.

To implement the mapping above, preprocessing of the shape reconstruction dataset is required (Fig. 6 (b)). First, image processing is applied to the circular acrylic region visible in the raw image to determine the center pixel coordinates (u_c, v_c) and the radius of the ROI. Using this information, both the tactile and reference images are cropped to 311×311, and the pixel values outside the ROI are set to zero. Next, a difference image is obtained by subtracting the cropped tactile image from the cropped reference image and then converting it to a grayscale image. From the difference image, we extract the pixel position with the highest intensity variation along with its corresponding intensity variation value. These extracted values are then paired with the sensor-frame coordinates (R, θ) of the tip of the indenter. For training the MLP, a dataset of 33,803 pairs was split into training and test datasets in an 8:2 ratio. A small MLP model with three hidden layers (3-32-32-32-2) was constructed using ReLU activation, following a similar network structure as [33]. The model was trained for 100 epochs with a batch size of 64, using the mean squared error (MSE) loss function and a learning rate of 0.001.

C. Force Estimation

The force estimation of UVDtact is conducted in UV LED mode following the pipeline shown in the bottom dashed box of Fig. 4. For force estimation, Resnet was selected as the neural network, similar to [29]. The preprocessing of the force estimation dataset followed a process similar to that of the shape reconstruction dataset, where a difference image was obtained. A difference image was then resized to $224 \times 224 \times 1$ and paired with the corresponding 3-axis force values. Additionally, as shown in Fig. 5 (c), the dataset of these pairs was divided into training and test datasets based on the object. For training, the Resnet-18 implementation from the PyTorch library was used, with modifications to set the input channel of the first convolutional layer to 1 and the output channel of the fully connected layer to 3. The model was trained for 100 epochs with a batch size of 32, using the L1 loss function and a learning rate of 1×10^{-4}.

V. Experimental Results

A. Shape Reconstruction

To quantitatively evaluate shape reconstruction performance, we assessed the shape reconstruction test dataset. The mean and standard deviation of the L2 distance between the predicted and actual 3D coordinates were measured as 0.172 mm and 0.136 mm, respectively. In Fig. 7, the qualitative performance of shape reconstruction is demonstrated by pressing various objects at different locations on the sensor. The objects that made contact with the sensor included a metal ball, a bolt head with a groove, a connector head, bolt threads, and a multi-touch using a hand. The reconstructed point clouds effectively captured the features of these diverse objects. Since the sensor is compact, it frequently interacts with relatively larger objects; however, even in such cases, no significant distortions were observed, and the point cloud

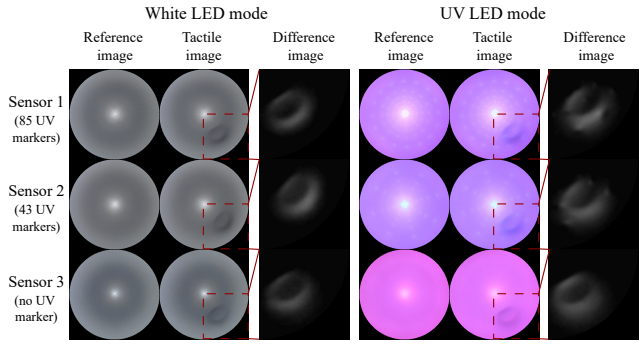

Fig. 8. Example reference, tactile, and difference images in white and UV LED modes for Sensors 1, 2, and 3.

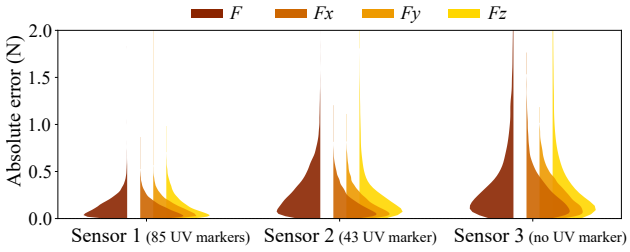

Fig. 9. Violin plots of force estimation results.

TABLE II

COMPARISON OF THE FORCE ESTIMATION PERFORMANCES

Sensor	Mean absolute error (N)			Standard deviation (N)		
	F_x	F_y	F_z	F_x	F_y	F_z
Sensor 1 (85 UV markers)	0.110	0.116	0.134	0.142	0.154	0.178
Sensor 2 (43 UV markers)	0.166	0.167	0.256	0.219	0.223	0.402
Sensor 3 (no UV marker)	0.266	0.239	0.384	0.333	0.298	0.645

was reconstructed while reflecting the geometric features of the object over a wide area. Additionally, due to the mapping method that incorporates geometric relationships, the sensor demonstrated consistent performance across contacts from various orientations.

B. Force Estimation

We conducted a force estimation performance evaluation to verify that the switchable translucent elastomer design enhances tactile feature richness in UV LED mode, improving force estimation accuracy, while preserving tactile image quality in white LED mode. To this end, in addition to the sensor with 85 UV markers implemented using the slot-and-protrusion structure, we also fabricated a sensor with 43 UV markers. Furthermore, a sensor without UV markers was produced by fabricating the inner and outer mixed elastomers at once using red UV ink. Example reference, tactile, and difference images of the fabricated sensors are shown in Fig. 8.

The force estimation results for the test objects are presented in Fig. 9 and Table 2. The sensor with 85 UV markers achieved an average mean absolute error (MAE) of 0.120 N

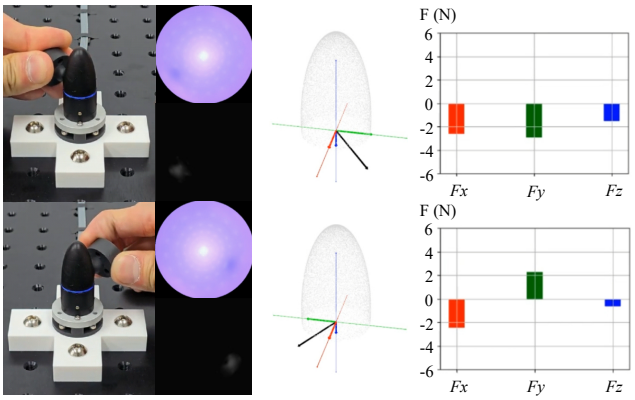

Fig. 10. Example of force estimation results for a test object captured in a real-time demonstration.

and an average standard deviation (Std) of 0.158 N. As the number of markers increased, the average MAE tended to decrease, with Sensor 1 exhibiting approximately a 60 % reduction in average MAE compared to Sensor 3. These results highlight that UVDtact enriches tactile features for force estimation by incorporating marker movement (Fig. 10). A denser arrangement of markers contributes to a more detailed representation, leading to improved force estimation. Furthermore, we confirmed that the markers embedded in the sensor are not visible in white LED mode, ensuring that the tactile images for shape reconstruction are not compromised (Fig. 8). Although force estimation performance could be further improved through different model architectures and marker arrangements, we focused on validating the effectiveness of this design.

VI. CONCLUSION

In this work, we present UVDtact, a vision-based tactile sensor with a fingertip-like form factor. By proposing a switchable translucent elastomer that combines UV ink with a translucent elastomer, the sensor selectively utilizes UV markers to enhance tactile features while leveraging the reflective properties of the translucent elastomer. This design supports uncompromised shape reconstruction and enhanced force estimation by ensuring that shape reconstruction remains unaffected by the markers while making them visible when necessary for force estimation. To achieve shape reconstruction in an all-around sensor configuration by leveraging translucency, a data-driven calibration method was adopted, and the shape reconstruction error was measured as 0.172 mm. Furthermore, the impact of UV markers on force estimation performance was validated by comparing elastomers with different marker configurations. A dense arrangement of UV markers resulted in a force estimation error of 0.120 N, marking a 60 % reduction compared to a configuration without markers. Notably, the placement of UV markers did not affect the quality of tactile images used for shape reconstruction.

Nevertheless, the proposed sensor has several drawbacks that need to be addressed. The sensor has a diameter of

18 mm, which is comparable to a human index finger but larger than a little finger. Achieving a more compact design would require selecting a smaller UV LED that still provides adequate illumination instead of the relatively large 3.5 mm diameter UV LED currently used. Additionally, integrating transfer learning capabilities, as demonstrated in [26], [29], is necessary to improve data efficiency. Future work will address the considerations mentioned above and utilize the integrated UVDtact with an anthropomorphic robotic hand to perform various dexterous object manipulation tasks.

REFERENCES

[1] R. S. Johansson and J. R. Flanagan, "Coding and use of tactile signals from the fingertips in object manipulation tasks," *Nature Reviews Neuroscience*, vol. 10, no. 5, pp. 345–359, 2009.

[2] G. Corniani and H. P. Saal, "Tactile innervation densities across the whole body," *Journal of Neurophysiology*, vol. 124, no. 4, pp. 1229–1240, 2020.

[3] Q. Li, O. Kroemer, Z. Su, F. F. Veiga, M. Kaboli, and H. J. Ritter, "A review of tactile information: Perception and action through touch," *IEEE Transactions on Robotics*, vol. 36, no. 6, pp. 1619–1634, 2020.

[4] R. S. Dahiya, P. Mittendorfer, M. Valle, G. Cheng, and V. J. Lumelsky, "Directions toward effective utilization of tactile skin: A review," *IEEE Sensors Journal*, vol. 13, no. 11, pp. 4121–4138, 2013.

[5] J. Zhang, H. Yao, J. Mo, S. Chen, Y. Xie, S. Ma, R. Chen, T. Luo, W. Ling, L. Qin, *et al.*, "Finger-inspired rigid-soft hybrid tactile sensor with superior sensitivity at high frequency," *Nature communications*, vol. 13, no. 1, p. 5076, 2022.

[6] S. Sundaram, P. Kellnhofer, Y. Li, J.-Y. Zhu, A. Torralba, and W. Matusik, "Learning the signatures of the human grasp using a scalable tactile glove," *Nature*, vol. 569, no. 7758, pp. 698–702, 2019.

[7] T. M. Huh, H. Choi, S. Willcox, S. Moon, and M. R. Cutkosky, "Dynamically reconfigurable tactile sensor for robotic manipulation," *IEEE Robotics and Automation Letters*, vol. 5, no. 2, pp. 2562–2569, 2020.

[8] X. Wang, L. Dong, H. Zhang, R. Yu, C. Pan, and Z. L. Wang, "Recent progress in electronic skin," *Advanced Science*, vol. 2, no. 10, p. 1500169, 2015.

[9] U. Kim, D. Jung, H. Jeong, J. Park, H.-M. Jung, J. Cheong, H. R. Choi, H. Do, and C. Park, "Integrated linkage-driven dexterous anthropomorphic robotic hand," *Nature communications*, vol. 12, no. 1, pp. 1–13, 2021.

[10] K. Shimonomura, "Tactile image sensors employing camera: A review," *Sensors*, vol. 19, no. 18, p. 3933, 2019.

[11] A. C. Abad and A. Ranasinghe, "Visuotactile sensors with emphasis on gelsight sensor: A review," *IEEE Sensors Journal*, vol. 20, no. 14, pp. 7628–7638, 2020.

[12] W. Yuan, S. Dong, and E. H. Adelson, "Gelsight: High-resolution robot tactile sensors for estimating geometry and force," *Sensors*, vol. 17, no. 12, p. 2762, 2017.

[13] B. Ward-Cherrier, N. Pestell, L. Cramphorn, B. Winstone, M. E. Giannaccini, J. Rossiter, and N. F. Lepora, "The tactip family: Soft optical tactile sensors with 3d-printed biomimetic morphologies," *Soft robotics*, vol. 5, no. 2, pp. 216–227, 2018.

[14] D. Ma, E. Donlon, S. Dong, and A. Rodriguez, "Dense tactile force estimation using gelslim and inverse fem," in *2019 International Conference on Robotics and Automation (ICRA)*. IEEE, 2019, pp. 5418–5424.

[15] Y. Du, G. Zhang, Y. Zhang, and M. Y. Wang, "High-resolution 3-dimensional contact deformation tracking for fingervision sensor with dense random color pattern," *IEEE Robotics and Automation Letters*, vol. 6, no. 2, pp. 2147–2154, 2021.

[16] W. Kim, W. D. Kim, J.-J. Kim, C.-H. Kim, and J. Kim, "Uvtac: Switchable uv marker-based tactile sensing finger for effective force estimation and object localization," *IEEE Robotics and Automation Letters*, vol. 7, no. 3, pp. 6036–6043, 2022.

[17] C. Lin, Z. Lin, S. Wang, and H. Xu, "Dtact: A vision-based tactile sensor that measures high-resolution 3d geometry directly from darkness," in *2023 IEEE International Conference on Robotics and Automation (ICRA)*. IEEE, 2023, pp. 10 359–10 366.

[18] W. Fan, H. Li, W. Si, S. Luo, N. Lepora, and D. Zhang, "Vitactip: Design and verification of a novel biomimetic physical vision-tactile fusion sensor," in *2024 IEEE International Conference on Robotics and Automation (ICRA)*. IEEE, 2024, pp. 1056–1062.

[19] H. Li, S. Nam, Z. Lu, C. Yang, E. Psomopoulou, and N. F. Lepora, "Biotactip: A soft biomimetic optical tactile sensor for efficient 3d contact localization and 3d force estimation," *IEEE Robotics and Automation Letters*, 2024.

[20] Z. Lu, J. Yang, H. Li, Y. Li, W. Si, N. Lepora, and C. Yang, "Tacshade: a new 3d-printed soft optical tactile sensor based on light, shadow and greyscale for shape reconstruction," in *2024 IEEE International Conference on Robotics and Automation (ICRA)*. IEEE, 2024, pp. 17 153–17 159.

[21] J. Jiang, X. Zhang, D. F. Gomes, T.-T. Do, and S. Luo, "Rotipbot: Robotic handling of thin and flexible objects using rotatable tactile sensors," *IEEE Transactions on Robotics*, 2025.

[22] Z. Chen, N. Ou, X. Zhang, and S. Luo, "Transforce: Transferable force prediction for vision-based tactile sensors with sequential image translation," *arXiv preprint arXiv:2409.09870*, 2024.

[23] I. H. Taylor, S. Dong, and A. Rodriguez, "Gelslim 3.0: High-resolution measurement of shape, force and slip in a compact tactile-sensing finger," in *2022 International Conference on Robotics and Automation (ICRA)*. IEEE, 2022, pp. 10 781–10 787.

[24] G. Zhang, Y. Du, H. Yu, and M. Y. Wang, "Deltact: A vision-based tactile sensor using a dense color pattern," *IEEE Robotics and Automation Letters*, vol. 7, no. 4, pp. 10 778–10 785, 2022.

[25] C. Lin, H. Zhang, J. Xu, L. Wu, and H. Xu, "9dtact: A compact vision-based tactile sensor for accurate 3d shape reconstruction and generalizable 6d force estimation," *IEEE Robotics and Automation Letters*, 2023.

[26] W. K. Do, B. Jurewicz, and M. Kennedy, "Densetact 2.0: Optical tactile sensor for shape and force reconstruction," in *2023 IEEE International Conference on Robotics and Automation (ICRA)*. IEEE, 2023, pp. 12 549–12 555.

[27] I. Andrussow, H. Sun, K. J. Kuchenbecker, and G. Martius, "Minsight: A fingertip-sized vision-based tactile sensor for robotic manipulation," *Advanced Intelligent Systems*, vol. 5, no. 8, p. 2300042, 2023.

[28] M. H. Tippur and E. H. Adelson, "Gelsight360: An omnidirectional camera-based tactile sensor for dexterous robotic manipulation," in *2023 IEEE International Conference on Soft Robotics (RoboSoft)*. IEEE, 2023, pp. 1–8.

[29] O. Azulay, N. Curtis, R. Sokolovsky, G. Levitski, D. Slomovik, G. Lilling, and A. Sintov, "Allsight: A low-cost and high-resolution round tactile sensor with zero-shot learning capability," *IEEE Robotics and Automation Letters*, vol. 9, no. 1, pp. 483–490, 2023.

[30] M. H. Tippur and E. H. Adelson, "Rainbowsight: A family of generalizable, curved, camera-based tactile sensors for shape reconstruction," in *2024 IEEE International Conference on Robotics and Automation (ICRA)*. IEEE, 2024, pp. 1114–1120.

[31] K. Vlack, T. Mizota, N. Kawakami, K. Kamiyama, H. Kajimoto, and S. Tachi, "Gelforce: a vision-based traction field computer interface," in *CHI'05 extended abstracts on Human factors in computing systems*, 2005, pp. 1154–1155.

[32] A. Yamaguchi and C. G. Atkeson, "Implementing tactile behaviors using fingervision," in *2017 IEEE-RAS 17th International Conference on Humanoid Robotics (Humanoids)*. IEEE, 2017, pp. 241–248.

[33] S. Wang, Y. She, B. Romero, and E. Adelson, "Gelsight wedge: Measuring high-resolution 3d contact geometry with a compact robot finger," in *2021 IEEE International Conference on Robotics and Automation (ICRA)*. IEEE, 2021, pp. 6468–6475.

[34] J. Di, Z. Dugonjic, W. Fu, T. Wu, R. Mercado, K. Sawyer, V. R. Most, G. Kammerer, S. Speidel, R. E. Fan, *et al.*, "Using fiber optic bundles to miniaturize vision-based tactile sensors," *IEEE Transactions on Robotics*, 2024.

[35] H. Sun, K. J. Kuchenbecker, and G. Martius, "A soft thumb-sized vision-based sensor with accurate all-round force perception," *Nature Machine Intelligence*, vol. 4, no. 2, pp. 135–145, 2022.

[36] W. K. Do and M. Kennedy, "Densetact: Optical tactile sensor for dense shape reconstruction," in *2022 International Conference on Robotics and Automation (ICRA)*. IEEE, 2022, pp. 6188–6194.

[37] J. W. Garrett, "The adult human hand: some anthropometric and biomechanical considerations," *Human factors*, vol. 13, no. 2, pp. 117–131, 1971.

[38] M. Murai, H.-K. Lau, B. P. Pereira, and R. W. Pho, "A cadaver study on volume and surface area of the fingertip," *The Journal of hand surgery*, vol. 22, no. 5, pp. 935–941, 1997.